İTÜ
MAKİNA FAKÜLTESİ
MAKİNA MÜHENDİSLİĞİ BÖLÜMÜ

CFD ANALYSIS OF AN INDUSTRIAL AXIAL FAN

SENIOR DESIGN PROJECT

Prepared By

030050019 Adem CANDAŞ
030050165 Hasan Erkan ÇELİKER
030060018 Ersin ÖZBALABAN

Supervisor

Prof. Dr. İlyas Bedii Özdemir

SPRING
2009-2010

CFD ANALYSIS OF AN INDUSTRIAL AXIAL FAN

Prepared By

030050019 Adem CANDAŞ
030050165 Hasan Erkan ÇELİKER
030060018 Ersin ÖZBALABAN

Supervisor

Prof. Dr. İlyas Bedii Özdemir

SPRING
2009-2010

FOREWORD

First of all, we would like to thank to all the people who supported us and were involved in one way or another in the preparation of this thesis. We would like to thank to our thesis supervisor Prof. Dr. I. Bedii ÖZDEMİR for giving us the opportunity to join his group and for his support.

Specially, we wish to thank our office-mates, Hande, Özer and Hayri. We are grateful for their interest in our work, friendship, cooperation and help.

Also, we thank to Taşkın Vantilatör ve Klima San. Tic. Ltd. Şti. for manufacturing of the fan blades.

Eventually, we are grateful to our families for their support, love and encouragement.

MAY 2010   Adem Candaş

Hasan Erkan Çeliker

Ersin Özbalaban

TABLE OF CONTENTS

ABBREVIATIONS

CAD : Computer Aided Design

CFD : Computational Fluid Dynamics

LES : Large Eddy Simulation

IGES : Initial Graphics Exchange Specification

LIST OF SYMBOLS

ω : Angular velocity (rpm)

D : Fan diameter

U_{mean} : Mean flow velocity scale

L_{mean} **:** Mean flow length scale

Re_{mean} **:** Reynolds number of mean flow

v **:** Kinematic viscosity of air (m^2/s)

U_0 **:** Velocity scale of the large eddies

L_0 **:** Length scale of the large eddies

τ_0 **:** Time scale of the large eddies

Re_0 **:** Reynolds number of the large eddies

λ **:** Length scale of the Kolmogorov eddies

U_λ **:** Velocity scale of the Kolmogorov eddies

τ_λ **:** Time scale of the Kolmogorov eddies

Δt **:** Time step of LES

LIST OF FIGURES

LIST OF TABLES

CFD ANALYSIS OF AN INDUSTRIAL AXIAL FAN

SUMMARY

Fans with improper intake geometry suffer from poor inflow conditions such as asymmetric velocity profiles and fluctuations leading increase in unsteady forces acting on blades. With proper blade profile, low-noise conditions can be obtained without giving up high aerodynamic performance.

In this study, performance of an axial flow fan is numerically examined by using LES and k-ε turbulence models. After creation of solid model out of point cloud, computational flow field is discretized using unstructured grids for both rotating and stationary domains. Rotation is defined between two domains by sliding mesh model. In order to observe the effect of pressure rise on flow rate, calculations are carried out for five pressure values: 80 Pa, 90 Pa, 100 Pa, 110 Pa and 120 Pa. Using flow rates corresponding to these pressure rises, performance curve of the fan is formed. Using a commercial CFD code, FLUENT, computations are done for two rotational speeds, 720 rpm and 1080 rpm. Thus, effect of rotational speed on flow rate is investigated for each pressure rise.

Finally, structural analysis is performed to examine the mechanical endurance of the fan. Static analysis is carried out on one blade under operating conditions 100 Pa and 720 rpm.

ENDÜSTRİYEL BİR EKSENEL FANIN HAD ANALİZİ

ÖZET

Fanlarda çalkantının oluşmasının sebebi, akışın kanat üzerinde ilerlemesi sırasında, bir bölümünün kanat profilini izleyemeyerek yüzeyden ayrılmasıdır. Uygun kanat profilleri kullanılarak yüksek aerodinamik becerinin yanı sıra düşük gürültülü çalışma koşulları da sağlanır.

Bu çalışmada, LES ve k-ε türbülans modelleri kullanılarak eksenel bir fanın performansı sayısal olarak incelenmiştir. Nokta bulutundan katı modelin oluşturulmasının ardından, ticari bir HAD koduyla hesaplamalı akış hacmi yapısal olmayan ağ kullanılarak sonlu elemana ayrılmıştır. Yapısal olmayan ağ dönen ve sabit hacim için ayrı ayrı oluşturulmuş, bu iki hakim arasındaki dönme hareketi kayar ağ örgüsü modeli ile tanımlanmıştır. Basınç artışının debi üzerindeki etkisini incelemek amacıyla hesaplamalar 5 farklı basınç artışı için yapılmıştır: 80 Pa, 90 Pa, 100 Pa, 110 Pa and 120 Pa. Elde edilen farklı debi ve basınç değerleri ışığında fanın performans eğrisi oluşturulmuştur. FLUENT kullanılarak yapılan hesaplamalarda, açısal hızın debi üzerindeki etkisi, 720 rpm ve 1080 rpm olmak üzere iki farklı açısal hız değeri için incelenmiştir. Böylelikle, her basınç değeri için iki farklı açısal hızdaki debi değeri bulunmuştur.

Son olarak, fanın mekanik dayanımı belirlemek için yapısal analiz uygulanmıştır. Statik analiz 720 rpm ve 100 Pa çalışma koşullarında tek bir kanat üzerinde yapılmıştır.

1. INTRODUCTION

Axial flow fans have wide spread usage from heavy industry applications to computer cooling systems. Hence design of axial fans became more important in recent years due to performance and noise issues. In general, high pressure rises or high flow rates are desired depending on the application. Therefore while high pressure with a reasonable flow rate is provided, noise level must be considered. Main source of noise generated in an axial flow fan is mainly on aerodynamic loads on fan blades. Fans with improper intake geometry suffer from poor inflow conditions such as asymmetric velocity profiles and fluctuations leading increase in unsteady forces acting on blades. In other words, with proper blade profile, low-noise conditions can be obtained without giving up high aerodynamic performance.

In this study, point cloud created by Özdemir [1] is converted into solid model in CAD format and then flow field is defined by computational grids. Using k-ε and LES are used as turbulence models, simulations are carried out for different rotational speeds and pressure rises in order to determine fan performance.

1.1. Axial Flow Fans

Axial flow fans are the types of fans that the fluid flow is mostly axial, parallel to axis of rotation. Axial flow fans usually use air as the working fluid that operates in incompressible range, at low speeds and moderate pressures. In an axial flow fan, the flow is ideally axial, with no radial component, and the required pressure rise comes from the increase in the tangential velocity component due to rotation of the impeller and an aerodynamic diffusion process afterwards. Since each application demands a different type, specific fans are more appropriate than others in terms of capacity and pressure rise capabilities. In this sense, axial flow fans are generally categorized into four types.

1.2. Axial Flow Fan Types

1.2.1. Propeller Fans

Propeller fans, also known as panel fans, are the most commonly used ones among axial flow fans, which are also lightest and cheapest in their genre. This leads propeller fans to be used in most of the applications, such as institutional and industrial i.e. exhaustion of corrosive gasses out of factories [2]. Therefore, propeller fans are built on the basis of blowing huge air volumes against low static pressures[3]. Construction of propellers are possible both direct drive and belt drive, as shown in the figure. In direct-drive type, rotation is carried from motor shaft to the fan wheel by an electric motor which is directly mounted to the fan wheel. On the other hand, stimulation is handled by belt-pulley arrangement in ,so called, belt drive propellers[2]. As both type has particular advantages, they have disadvantages, as well. For instance, since having less component and saving the energy amount expended by belt and pulley configuration, direct drive seems cheaper and more appropriate. On the contrary, considering pulley ratio and its ability to vary, belt-drive type provides better performance flexibility. However, having flexibility in performance is possible in direct-drive, by the usage of adjustable pitch on blades.

To conclude, direct drive is less expensive and more efficient. It is more suitable in small sizes. Belt drive is preferable in large sizes and results better performance flexibility than direct drive, unless adjustable-pitch blades are used.

a)   b)
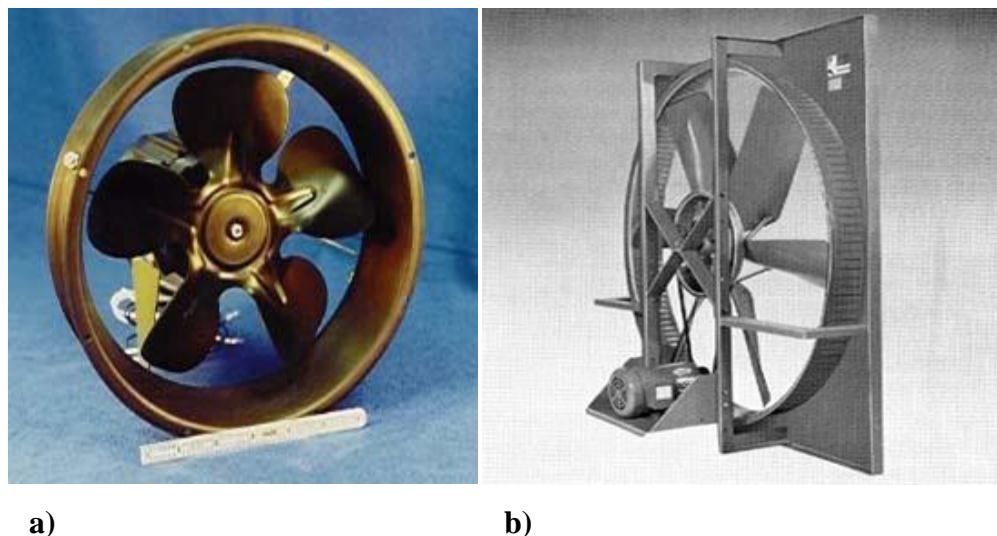
Figure 1.1: Propeller Fans; a)Direct drive, b)Belt drive

1.2.2. Tube Axial Fans

Tube axial fans are propeller fans placed in a cylinder when the air is desired to enter and leave the blading in axial direction. Comparing with propellers, it is possible to obtain higher pressures and better operating efficiencies with tube-axial fans [3]. Exhausting from inlet duct seems to be the best application for this type, because using outlet ducts leads pressure losses after the fan wheel due to the air spin existence [3]. On the other hand, being relatively expensive and low energy efficiency is considered to be disadvantages of tube-axials.

Figure 1.2: Tube-Axial Fan

1.2.3. Vane Axial Fans

A vane axial fan differs from a tube-axial for including downstream guide vanes. Guide vanes are used for neutralization of air spin which leads to rise in static pressure. That makes vane axials suitable for high pressure applications, however they are relatively expensive comparing the other fan types.
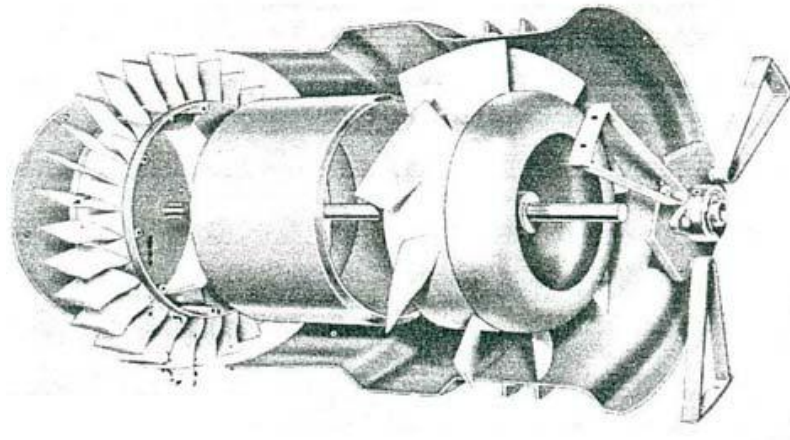
Figure 1.3: Vane-Axial Fan

1.2.4. Two Stage Fans

Two stage axial fans are used for higher static pressure applications. There are two different configuration to design a two-stage. In the first one, both fan wheels rotates in the same direction including guide vanes between them whereas two counter rotating fan wheels are used without guide vanes in the second one. By either configuration pressure is doubled [2]. In the first configuration, guide vanes behave as the outlet for the first stage and inlet for the second stage, because they get the flow generated by first stage, and neutralize it for the second stage. This one seems advantageous because same fan wheel shaft is used for both stages.
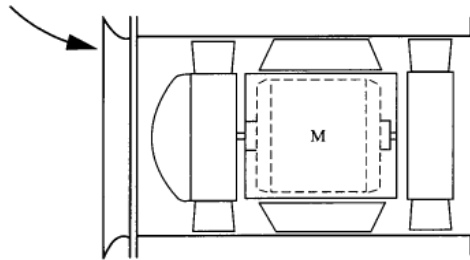
Figure 1.4: Two-Stage Fan, with first configuration

In the second configuration, fan wheels are driven by two different motors. Since no guide vanes are used, a reduction occurs in the payment for the second motor. With this configuration, in case of one of the motors' failure, the other one still works and blowing process continues.
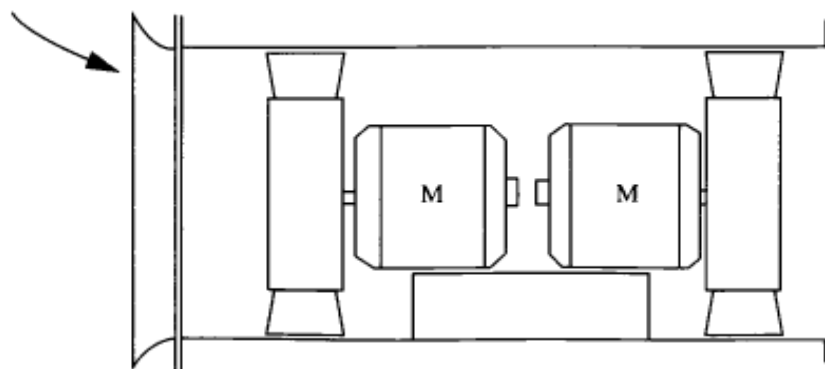
Figure 1.5: Two-Stage Fan, with second configuration

1.3. Performance of Axial Fans

Performance of an axial fan is qualified by various physical quantities such as static pressure, total pressure, flow rate, rotation speed, motor input, mechanical efficiency, static pressure efficiency, sound level, etc. However, static pressure and flow rate are mostly used performance criterias to characterize a fan [4]. Figure 1.6 shows a typical performance curve. Starting from the free delivery, the pressure value rises to a peak value. This is the good operating range for an axial flow fan. As the air volume decreases due to increasing restrictions, the axial air velocity decreases as well, resulting in an increased angle of attack and increased lift coefficients. The increase in the lift coefficient is responsible for the increase in the pressure. After the maximum lift angle is reached, the flow can no longer follow the upper contour of the blades, thus separate from the surface of the blade [5]. Separated flow results in a decrease in lift coefficient, thus a decrease in pressure occurs, which is called *stall* condition. After the stalling, the axial flow fan starts acting like an inefficient and noisy mixed flow fan. As the airflow approaches the fan inlet, the blades throw the air outward by centrifugal force and in this way produce the static pressures of the stalling range, which keeps until the point of no delivery is reached.
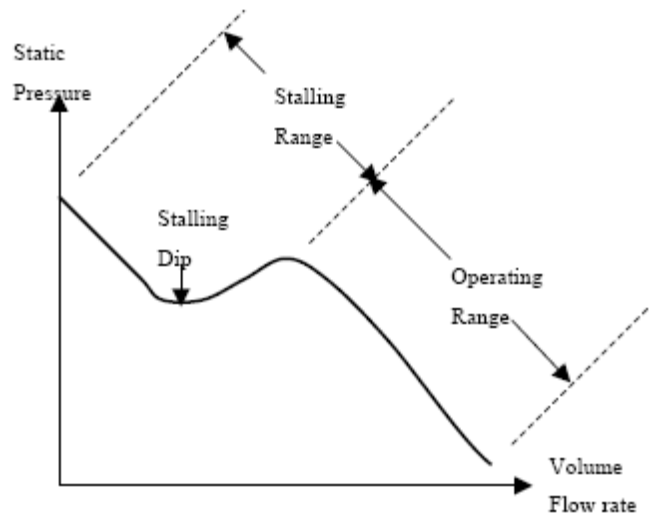
Figure 1.6: Fan Performance Curve [1]

Axial flow fans are designed for highest level of efficiency. However other levels of characteristics must be considered. Figure 1.7 shows different flow conditions for an axial fan. As it can be seen from the figure, at (d) the flow is uniform, while at other

conditions different vortex formations are observed. Noise level increases with growth of those formations.
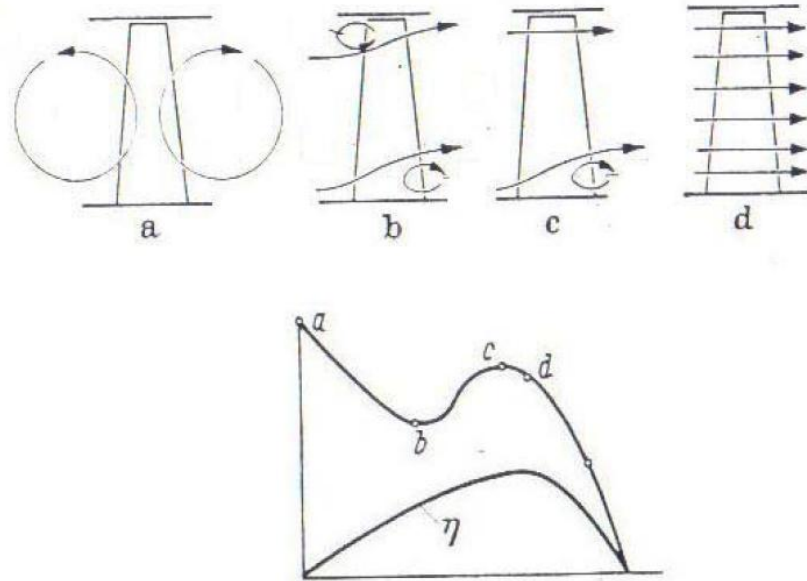
Figure 1.7: Diagrams of different flow conditions of an axial flow fan at different throttling positions [6]

2. CAD OBJECT AND GRID GENERATION

2.1. Cad Object

The point cloud of a single blade (Figure 2.1) given by Özdemir [1] is imported into a commercial software which is used to create 3D geometry.
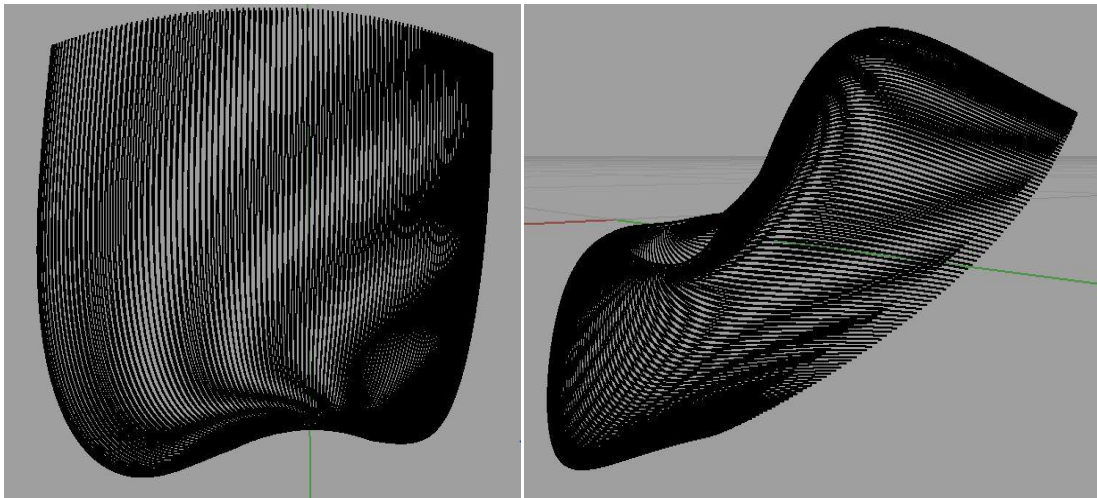
Figure 2.1: The cloud points of blade

The edge curves are created by combining points with line segments. Then the surface of the area between the curves is generated which is shown in Figure 2.2 and Figure 2.3.
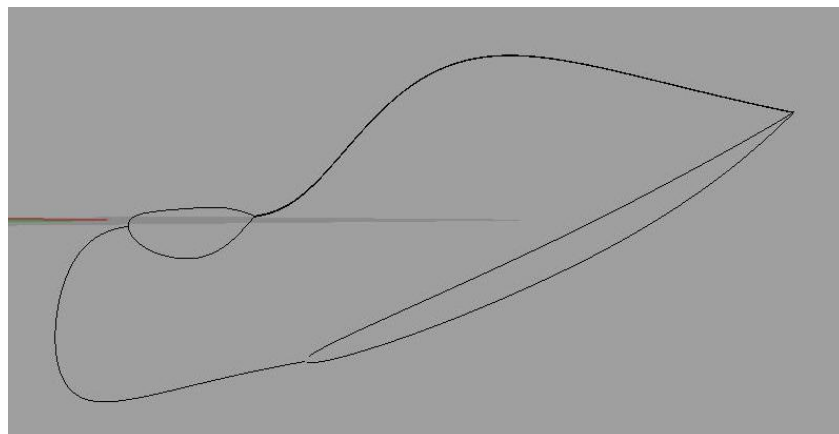
Figure 2.2: Edge curves of the blade
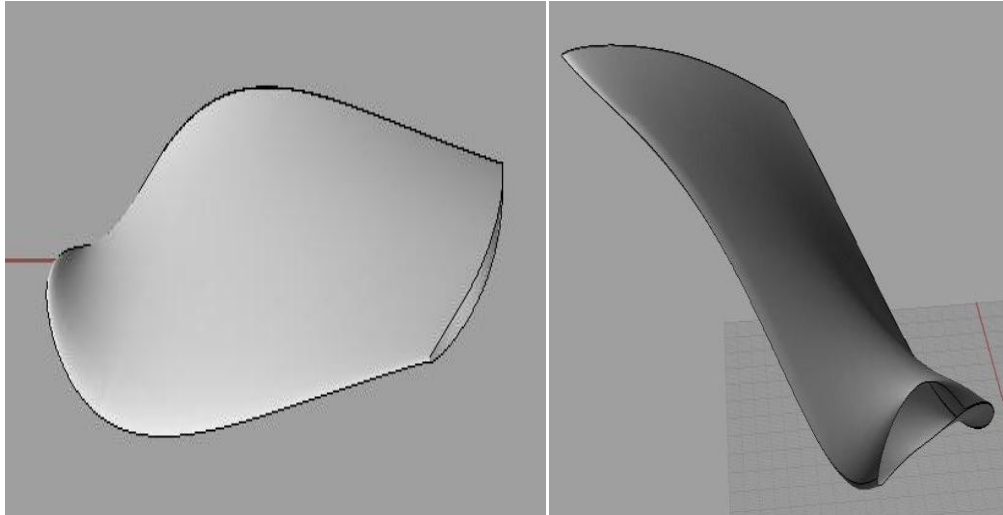
Figure 2.3: Blade 3D geometry

Once the surfaces are constructed, rotor part is formed as seen in Figure 2.4.
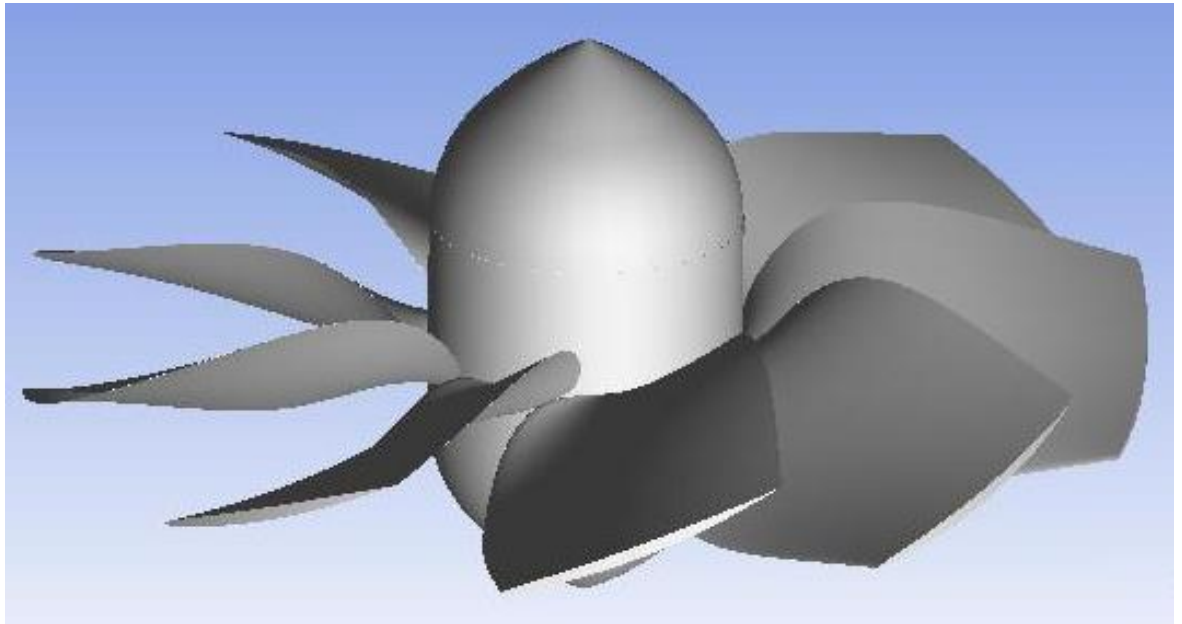
Figure 2.4: Rotor 3D geometry

To conduct numerical analysis, the rotor is surrounded by a round duct with the dimensions given in Table 2.1. The duct extends from an inlet section two diameter upstream of the fan to the outlet section which is one diameter downstream which secures streamlined flow at the inlet and outlet sections. It should be pointed out that the cross-section of the duct is enlarged at the inlet with the edges rounded as shown in Figure 2.5.

Table 2.1: Dimensions of the duct in mm

Inlet Diameter	152
Outlet Diameter	103
Length	5000
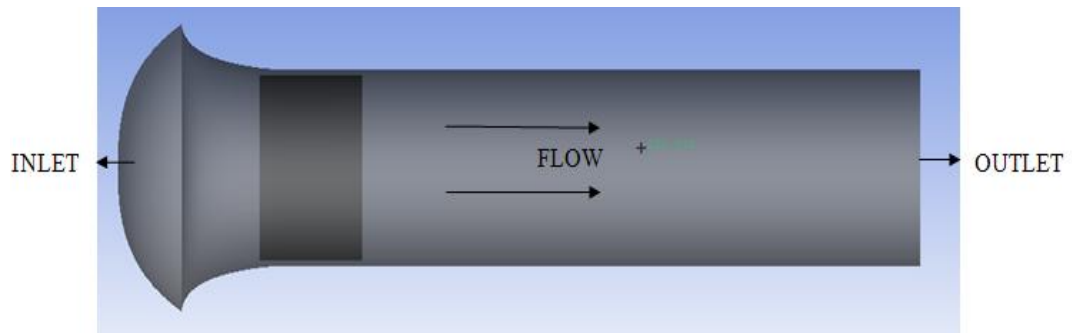
Figure 2.5: Duct geometry

2.2. Grid Generation

In CFD applications, computational flow field must be discretized into finite volumes in order to perform numerical calculations. The grid generation process is performed with Ansys ICEM CFD software package which has the capability to generate various types of grids such as hexagonal, tetrahedral, prismatic and quadratic. In this study, tetrahedral cells are used in computational flow field since they are more flexible and easy to apply on complex geometries such as blade geometries in this study. Figure 2.6 shows an example for unstructured grid type.
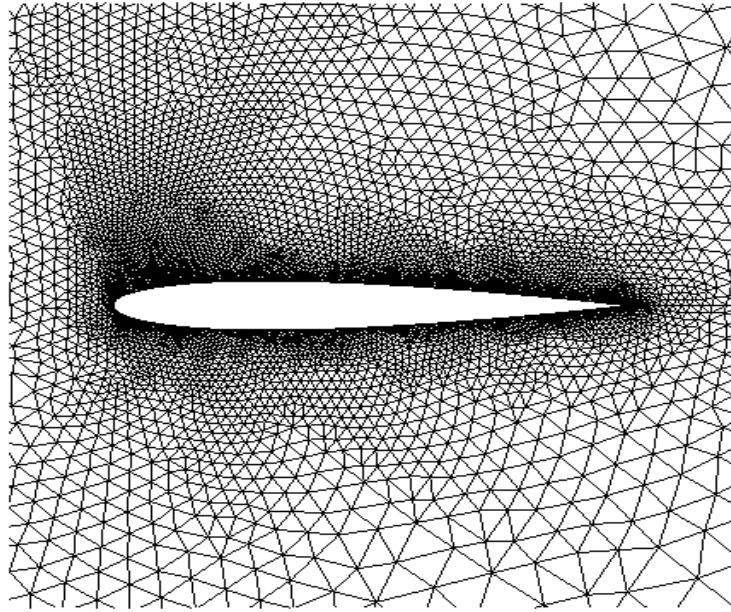
Figure 2.6: Unstructured grid

After CAD object is imported in ".igs" file format, a topology check is performed to check gaps in the geometry. This operation is necessary in order to have solid geometry fully enclosed so that the flow domain can be properly meshed separate from solid geometry. Once topology check is accomplished, geometry is then partitioned into related families. Since sliding mesh technique is used in this study, stationary and rotating domains are meshed separately. While AIR_ROT, ROTOR and REF_ROT families are defined for rotating domain, INLET, OUTLET, REF_STA, WALL and AIR_STA families are defined for stationary domain.
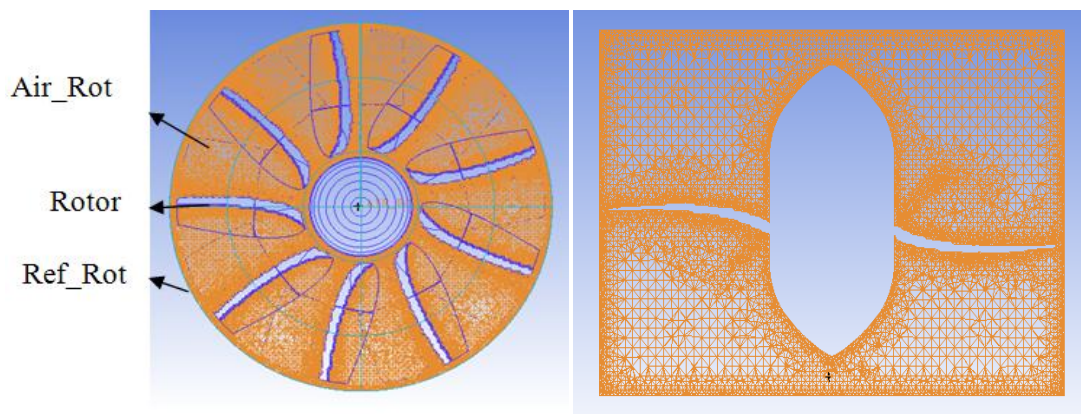
Figure 2.7: The grid of rotating domain

Table 2.2: Grid information for rotating domain

ELEMENT TYPE	ELEMENT NUMBER			
LINE	3221			
TETRA	1759575			
TRI	220204			
ELEMENT PARTS	ELEMENT NUMBER		TOTAL ELEMENT NUMBER	1983000
AIR_ROT	1759575			
REF_ROT	130975		TOTAL NODES	355998
ROTOR	92450			
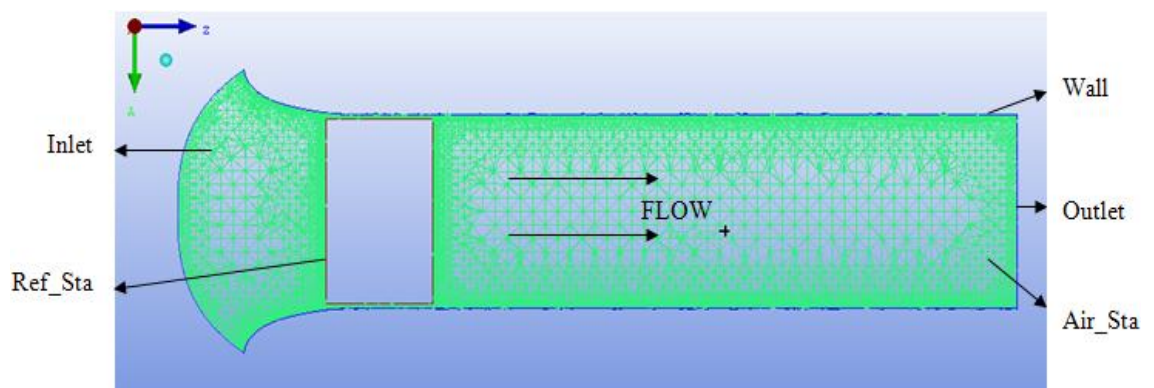
Figure 2.8: The grid of stationary domain

Table 2.3: Grid information for stationary domain

ELEMENT TYPE	ELEMENT NUMBER			
LINE	1515			
TETRA	1805629			
TRI	230608			
ELEMENT PARTS	ELEMENT NUMBER			
AIR_STA	1805629			
REF_STA	100531		TOTAL ELEMENT NUMBER	2037752
INLET	6411			
OUTLET	1967		TOTAL NODES	367323
WALL	123214			

11

3. COMPUTATIONAL FLUID DYNAMICS

Calculations are done using a commercial code, FLUENT. Firstly standard k-ε model and then LES is used as turbulence models. Simulation is done for different operation conditions; for different pressure rises at different rotational speeds.

3.1. Sliding Mesh Model

Since an axial fan has both stationary and rotating parts, rotation is needed to be defined in the computational flow field. There are models improved for defining rotation such as multiple reference frame model, mixing plane model and sliding mesh model. However, first and second models are applicable only for steady state flow problems. Since it is more suitable also for unsteady flow problems, sliding mesh model is applicable for LES applications [7]. Furthermore, as it does not require for remeshing at every time step, sliding mesh model is frequently used at computational turbomachinery applications [8]. In sliding mesh model, reference plane that split stationary and rotating domains must be exactly the same.
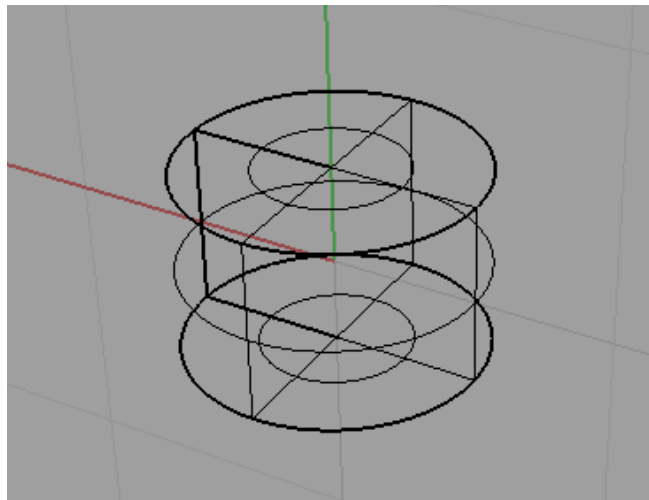
Figure 3.1: The reference plane
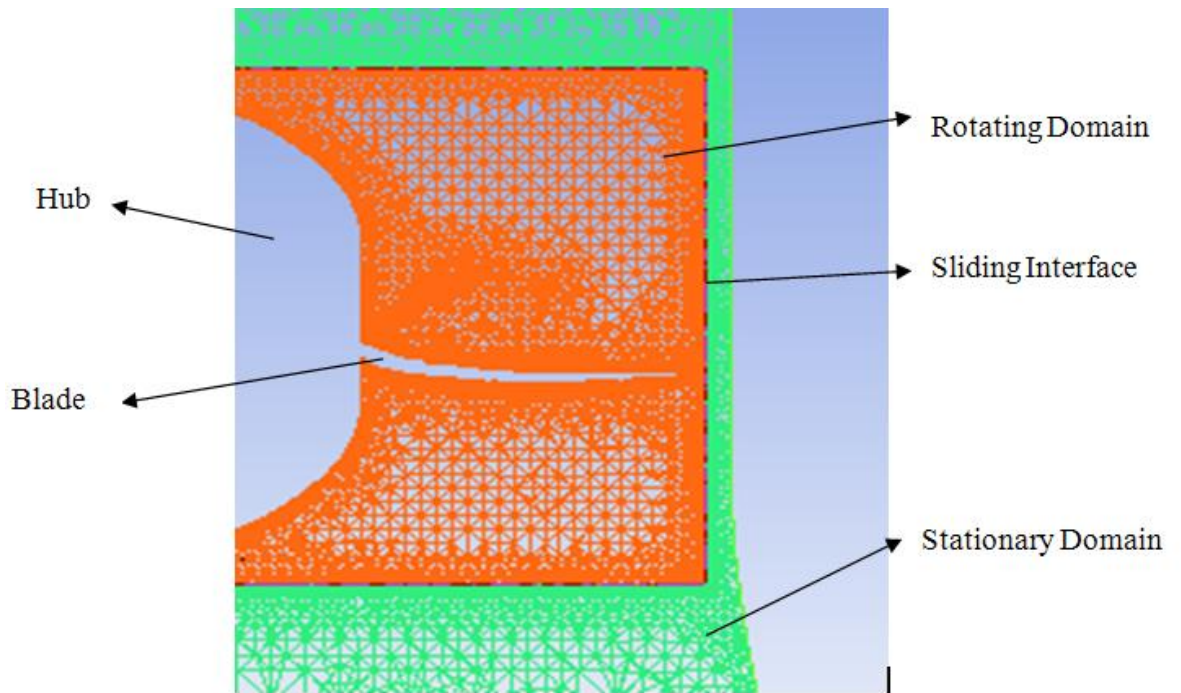
Figure 3.2: The sliding interface

Unstructured tetrahedral cells are used to define both computational domains. Mesh parameters are set for each family according to their mesh density requirements. On blades and reference planes, the mesh is finer in order to get more accurate increase accuracy on those zones. After enough iterations are done for mesh quality checks, output for both domain is saved in ".msh" file format. Before running calculations in the CFD code, the domains must be merged. This process is held by one of the FLUENT's utilities, TMERGE v2.1. Employing TMERGE v2.1 rotating and stationary domains are merged and converted into one ".msh" file.

3.2. Boundary Conditions:

When it comes to the assignment of the boundary conditions to related grid families created in meshing step, fluid domain of rotating part, AIR_ROT, is set as "moving mesh" with two different rotational speeds, 720 and 1080 rpm whereas AIR_STA is set as "stationary". Moreover, REF_STA and REF_ROT are set as "interface".
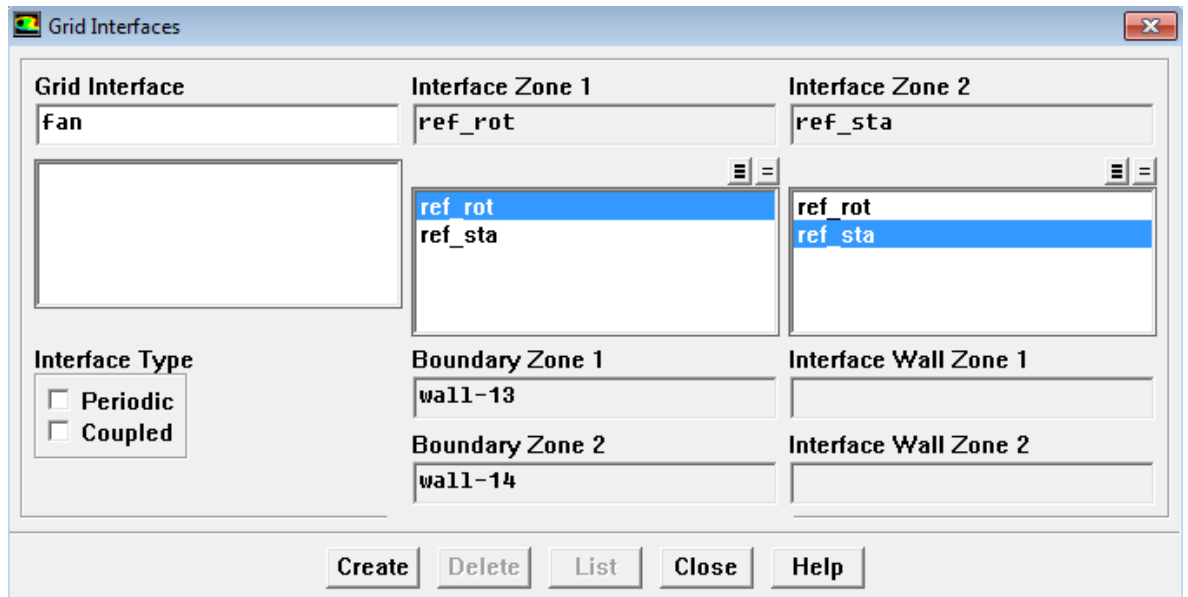
Figure 3.3: Grid Interfaces

INLET and OUTLET zones are assigned as "pressure inlet" and "pressure outlet" while WALL is set as "stationary wall". Outlet pressure is set different values to examine flow rate for each pressure value, those are 80 Pa, 90 Pa, 100 Pa, 110 Pa and 120 Pa. Outlet pressure is defined as static pressure, and inlet pressure is total pressure. Therefore, to keep inlet static pressure zero, total pressure at inlet is set to 1.5 ~ 2 Pa, corresponding to the dynamic pressure due to non-zero velocity at the inlet. Moreover, in order to keep inlet static pressure zero during calculations, velocity values at inlet are checked frequently and total inlet pressure is updated according to those velocity values as solution develops.

3.3. Turbulence

3.3.1. Turbulence Models

The small eddies receive the kinetic energies from slightly larger eddies which receive their energy from even larger eddies. And the largest eddies extract their energy from the mean flow. Kinetic energy in the small eddies are transformed into thermal energy due to high viscous forces in smaller eddies [9]. Transferring energy from larger eddies to small eddies is called the cascade process as seen schematically in Figure 3.4 and Figure 3.5.
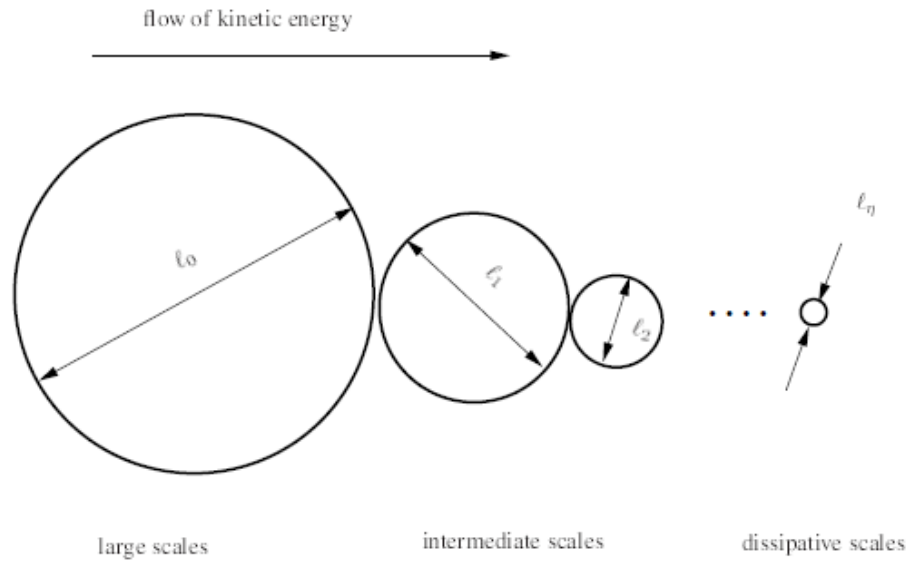
Figure 3.4: Cascade process with spectrum of eddies [10]
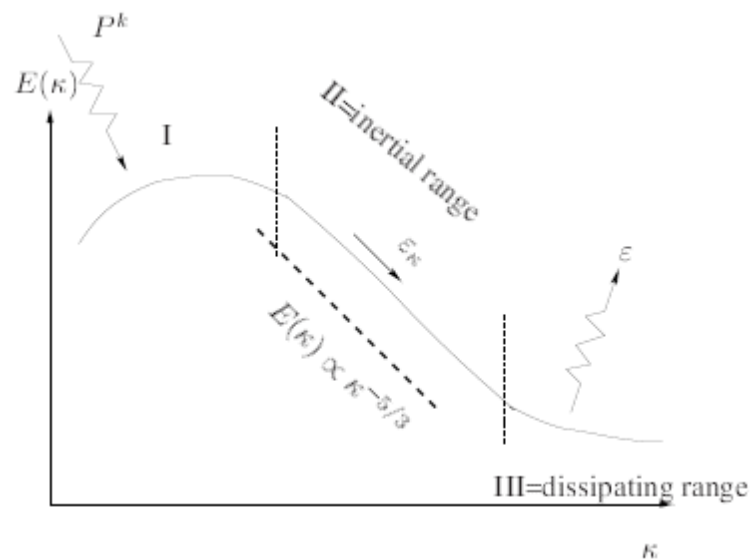
Figure 3.5: Spectrum for turbulent kinetic energy, k. I: Range for large, energy containing   eddies. II: The inertial subrange. III: Range for small scales [10]

In Figure 3.5 the regions correspond to;

I is the region, with the large eddies. These eddies, carrying most of the energy, interact with the mean flow and extract energy from the mean flow. II is called inertial subrange where the Reynolds number is high which means that flow is fully turbulent. The eddies in this region represent the mid-region which is a "transport region" in this cascade process. III is called dissipation range where the eddies are

15

small and isotropic and dissipation occurs. The energy transfer from turbulent kinetic energy to thermal energy which causes increase in temperature. The scales of the eddies are described by the Kolmogorov [11].

3.3.1.1. k-ε

The k-ε turbulence model is the most widely employed two-equation eddy-viscosity model which is a semi-empirical and based on model transport equations for the turbulence kinetic energy (k) and its dissipation rate (ε). The model transport equation for k is derived from the exact equation, while the model transport equation for ε was obtained using physical reasoning and bears little resemblance to its mathematically exact counterpart. In the derivation of the k-ε model, it was assumed that the flow is fully turbulent, and the effects of molecular viscosity are negligible. The standard k-ε model is therefore valid only for fully turbulent flows.

3.3.1.2. Large Eddy Simulation

LES captures the transient nature of the flow by spatially averaging and modeling on the sub-grid and in this way, LES provides the instantaneous results as does Direct Numerical Simulation, includes empirical modeling like Reynolds Averaged Navier-Stokes to be more efficient. The turbulence models for Reynolds Averaged Navier-Stokes are very much limited on the range of applications, because they attempt to model a wide range of scales and the random motion of eddies with no organized behavior [13].

In Large Eddy Simulation, small-scale turbulence is filtered out from the Navier-Stokes equations, and a model is used to evaluate small scales, schematically shown in the Figure 3.6. The resulting filtered Navier-Stokes equation is solved for the large scale motion. It is responsible for most of momentum and energy transport. The large scale of motion is highly dependent on the flow conditions and geometries under consideration. The small scales are computed from the turbulence model known as the sub-grid scale model. Since the small-scale eddies are more or less universal and homogeneous, it is accepted that the sub-grid scale model would be applicable to a wide range of flow regimes and conditions.
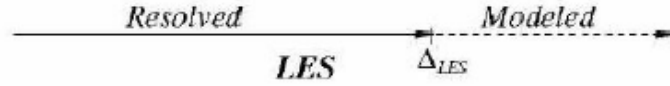
Figure 3.6: Modeling steps for LES turbulence model [12]

3.3.2. Turbulence Parameters

As mentioned above, energy is transferred from larger scales through smaller scales until viscosity losses its effect on. Kolmogorov scales are considered to be the smallest scales which mean no longer viscosity is effective and no dissipation exists. Relationships between small and larger scales are defined on the basis of Reynolds number.

For the mean flow, velocity scale can be assumed maximum velocity at the tip, which is calculated using (3.1).

$$U_{mean} = \omega \times \frac{D}{2} \tag{3.1}$$

U_{mean} is calculated as 37.7 [m/s] for 720 rpm and 56.6 [m/s] for 1080 rpm. Since length scale of the mean flow is the radius of the propeller 0.5 m [for] both rpm values.

$$L_{mean} = \frac{D}{2} = 0.5 \, [m] \tag{3.2}$$

Knowing L_{mean} and U_{mean}, Reynolds number can be calculated as 12.56 x10^5 for 720 rpm and 18.87 x10^5 for 1080 rpm, using (3.3).

$$Re_{mean} = \frac{U_{mean} \, L_{mean}}{\nu} \tag{3.3}$$

and this shows mean flow is fully turbulent. Here, ν is the kinematic viscosity of air, and it is 1.5 x10^{-5} [m^2/s]. There are two relations between the large scales and the mean flow scales. First one is that strain rates are proportional, and the second one is that Reynolds number of the mean flow is one order of magnitude greater than the Reynolds number of large eddies [15]. Using these assumptions length scale and

velocity scales can be derived and calculated as below. Here, U_o and L_o represents velocity and length scales of large eddies.

$$\frac{U_{mean}}{L_{mean}} = \frac{U_o}{L_o} \quad \Rightarrow \quad L_o = U_o \frac{L_{mean}}{U_{mean}} \tag{3.4}$$

$$Re_{mean} = 10 \times Re_o \quad \Rightarrow \quad \frac{U_{mean} \, L_{mean}}{\nu} = 10 \frac{U_o L_o}{\nu} \tag{3.5}$$

Using (3.4) and (3.5), relationship between U_{mean} and U_o can be determined as,

$$\frac{U_{mean} \, L_{mean}}{\nu} = 10 \frac{\frac{L_{mean}}{U_{mean}} U_o{}^2}{\nu} \quad \Rightarrow \quad U_{mean}{}^2 = 10 U_o{}^2 \tag{3.6}$$

Since U_{mean} is known, U_o is calculated as 11.9 [m/s] for 720 rpm and 17.9 [m/s] for 1080 rpm. And using (3.4), L_o is determined as 0.158 [m]. Hence time scale of large eddies is calculated as 1.3×10^{-2} [s] for 720 rpm and 0.88×10^{-2} [s] for 1080 rpm.

$$\tau_o = \frac{L_o}{U_o} \tag{3.7}$$

There is another relationship defined between length scales of Kolmogorov and large eddies.

$$\frac{\lambda}{L_o} = \frac{1}{(Re_o)^{3/4}} \tag{3.8}$$

where λ represents length scale of Kolmogorov eddies, and using (3.8) it is calculated as 2.36×10^{-5} [m] for 720 rpm and 1.7×10^{-5} [m] for 1080 rpm. In order to calculate time scale of Kolmogorov eddies, Reynolds number can be considered as nearly 1, $Re_\lambda \approx 1$. Assuming Reynolds number as 1, velocity scale, U_λ, can be calculated as 0.635 [m/s] for 720 rpm and 0.88 [m/s] for 1080 rpm. Then from $\tau_\lambda = \lambda/U_\lambda$ relation, time scale of Kolmogorov eddies, τ_λ, is calculated as 3.71×10^{-5} [s] for 720 rpm and 1.93×10^{-5} [s] for 1080 rpm.

In this study, time step size in FLUENT is taken about one order of magnitude greater than the Kolmogorov time scale to capture the lowest scales the inertial subrange [16]. For 720 rpm, it can be assumed as $\Delta t= 4 \times 10^{-4}$ [s]. With near assumption, it is $\Delta t= 2 \times 10^{-4}$ [s]. Since rotational speed is 720 rpm, fan makes 12 revolutions in a second, which means 210 iterations will be enough to simulate a full revolution of the fan considering time step size. Furthermore, when the rotational speed is 1080 rpm, fan makes 18 revolutions in a second, which means 280 iterations will be enough.
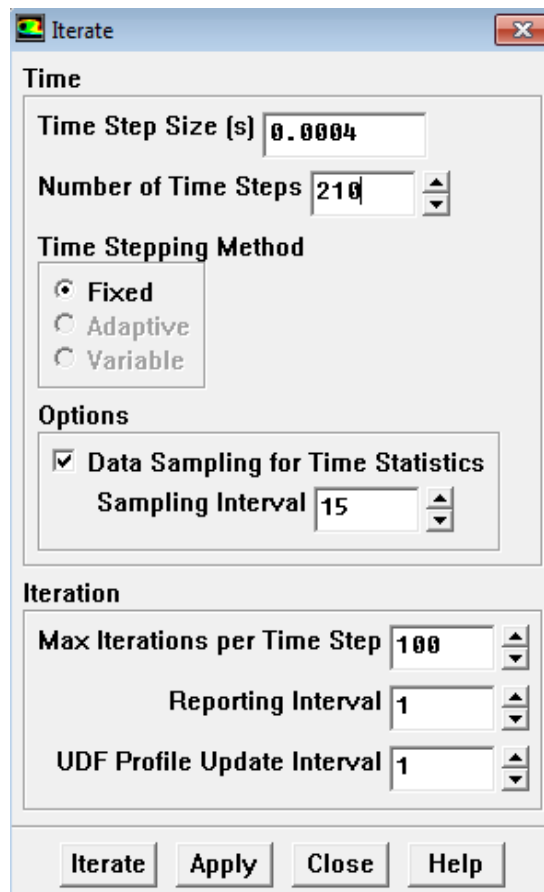
Figure 3.7: LES iteration panel for 720 rpm

4. RESULTS & DISCUSSION

4.1. CFD Analysis

All the velocity and pressure distributions are calculated on the axial fan for the given boundary conditions. Simulations are carried out for five pressure values: 80 Pa, 90 Pa, 100 Pa, 110 Pa and 120 Pa at two rotational speeds: 720 rpm and 1080 rpm. Output figures are exported for 100 Pa.
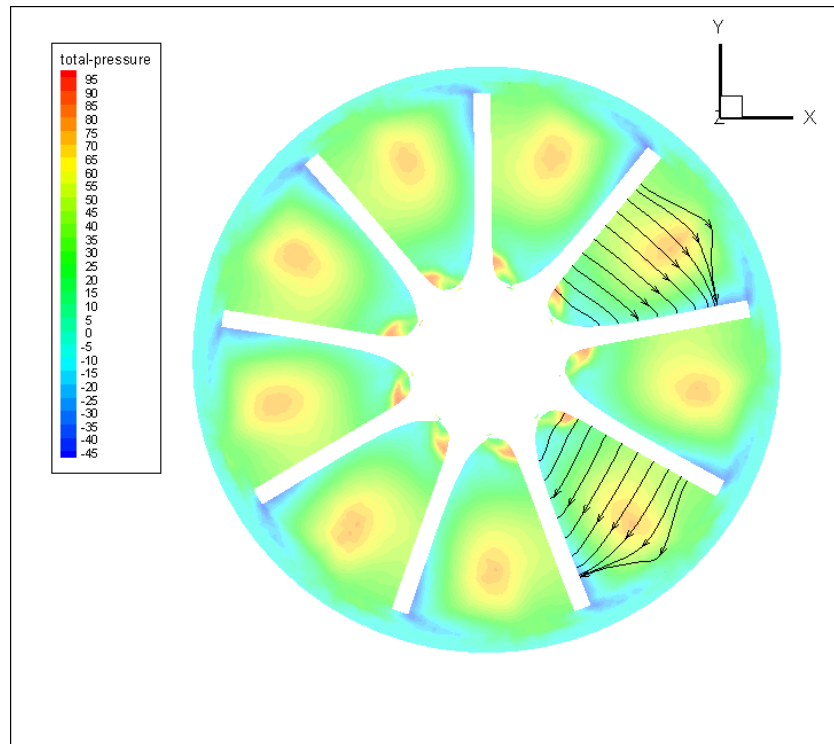
Figure 4.1: Total pressure distribution on XY plane at 720 rpm

In Figure 4.1 and Figure 4.2, total pressure distribution for both rotational speeds can be seen and it is observed that streamlines are moving through –z. Furthermore, in Figure 4.3 it is seen that flow vectors are uniform in the radial direction.
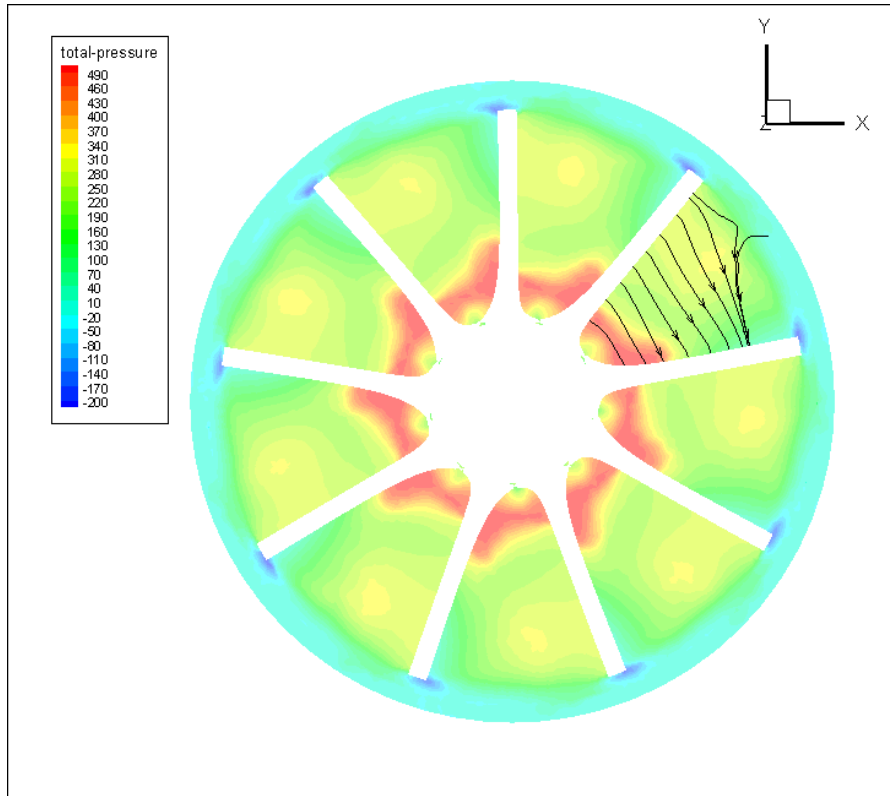
Figure 4.2: Total pressure distribution on XY plane at 1080 rpm
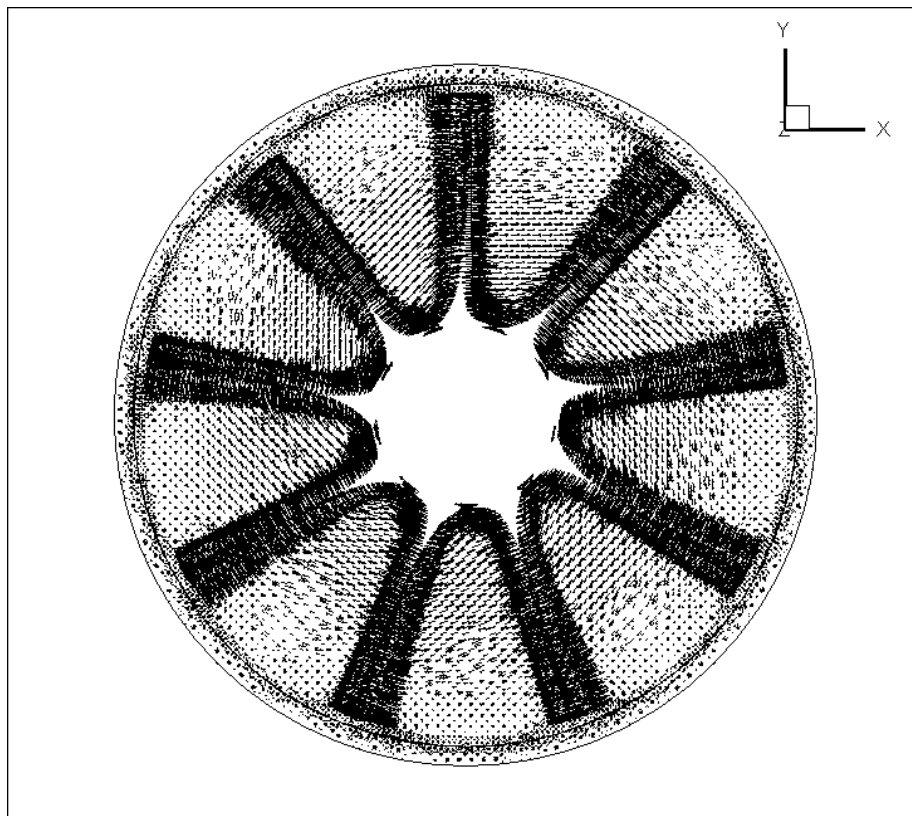
Figure 4.3: Flow vectors on XY plane at 720 rpm

21
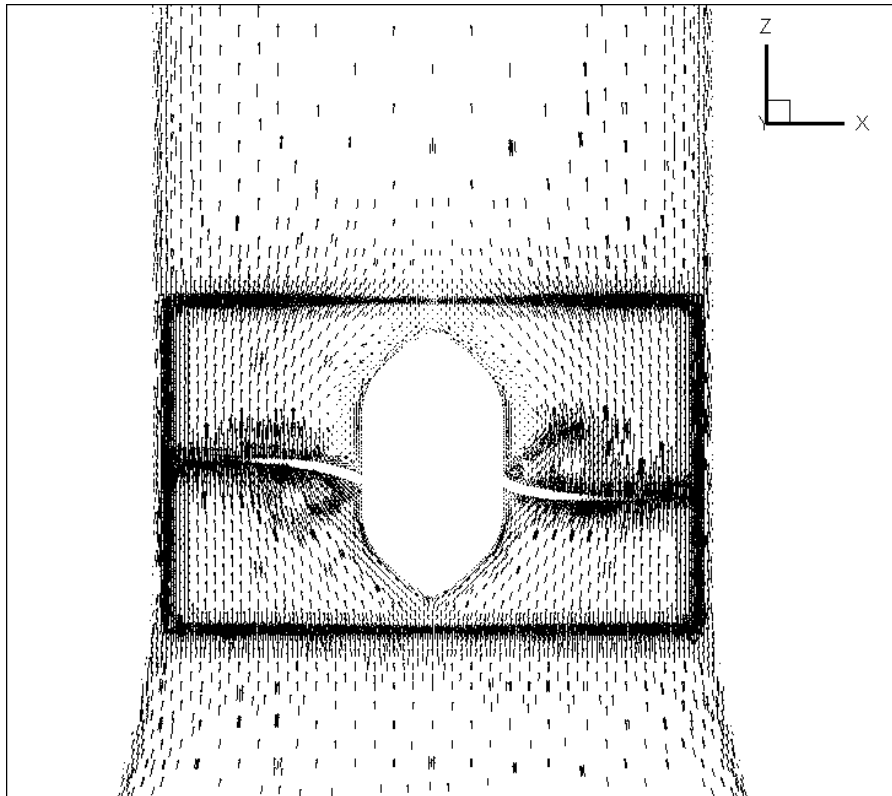
Figure 4.4: Flow vectors on XZ plane at 720 rpm
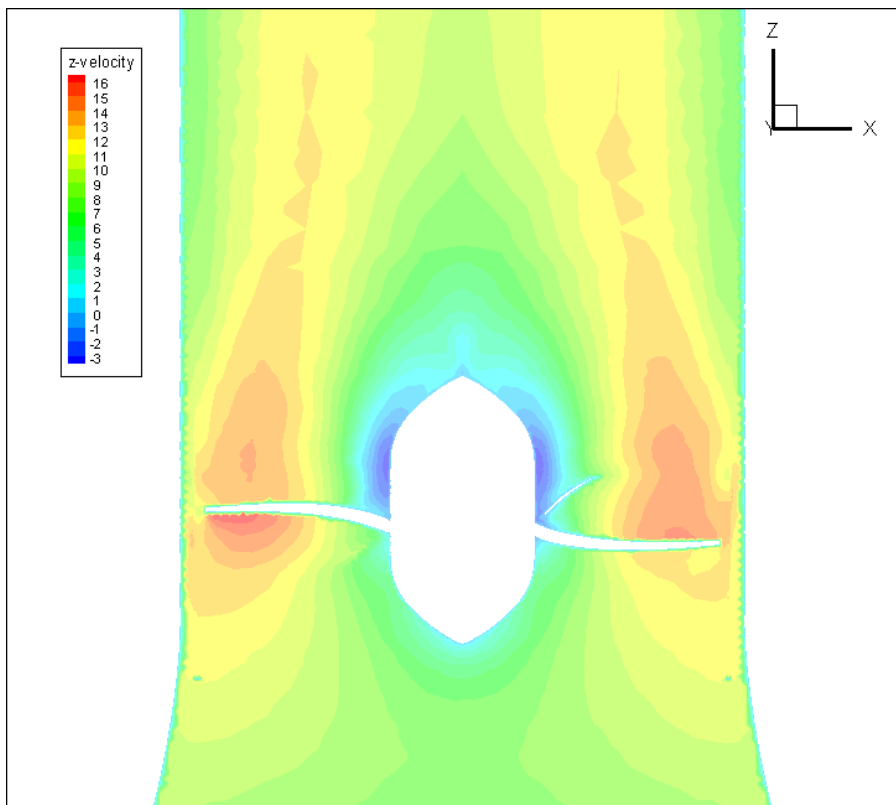
Figure 4.5: z-velocity distribution on XZ plane at 720 rpm
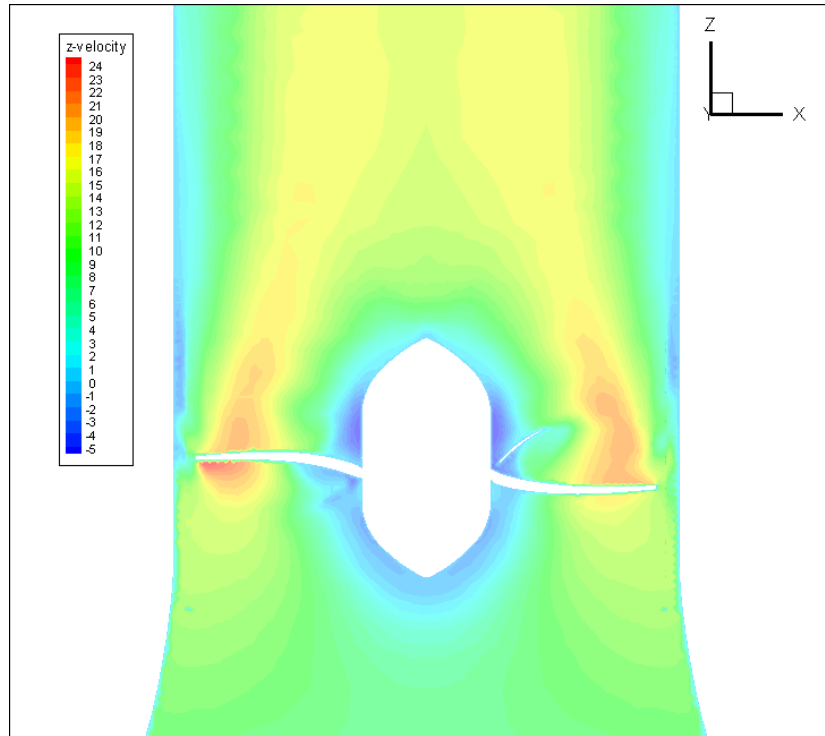
Figure 4.6: z-velocity distribution on XZ plane at 1080 rpm

In Figure 4.5 and Figure 4.6, z component of velocity distribution is seen and as expected, velocity values reach their maximum at the tip of the fan blades due to centrifugal forces.
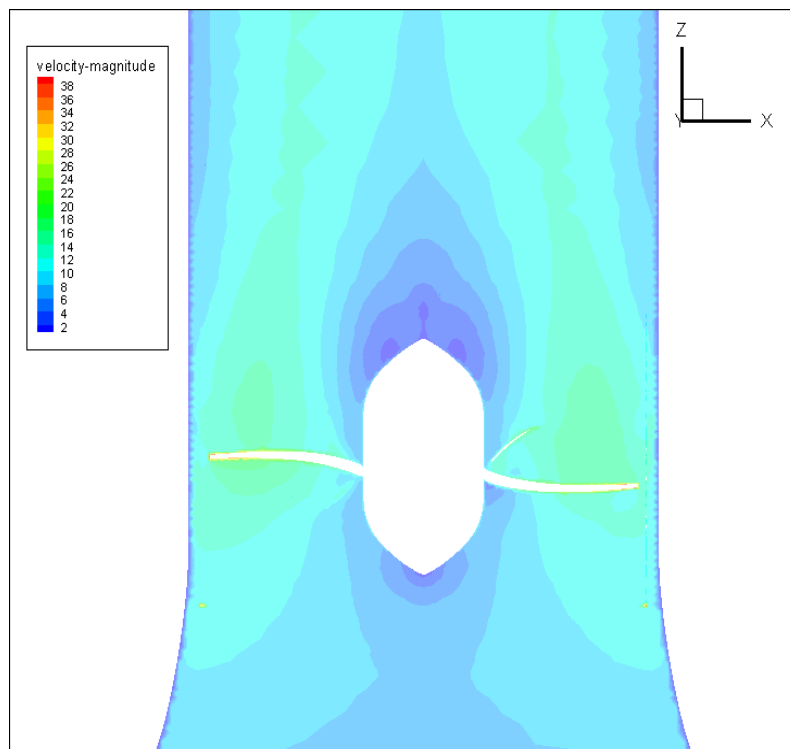
Figure 4.7: Velocity magnitude distribution on XZ plane at 720 rpm

Distribution of velocity magnitude on x-z plane can be seen in Figure 4.7 and Figure 4.8 for both rotational speeds. As mentioned above, velocity magnitude is maximum at the tip. After leaving the blade, velocity of the flow decreases.
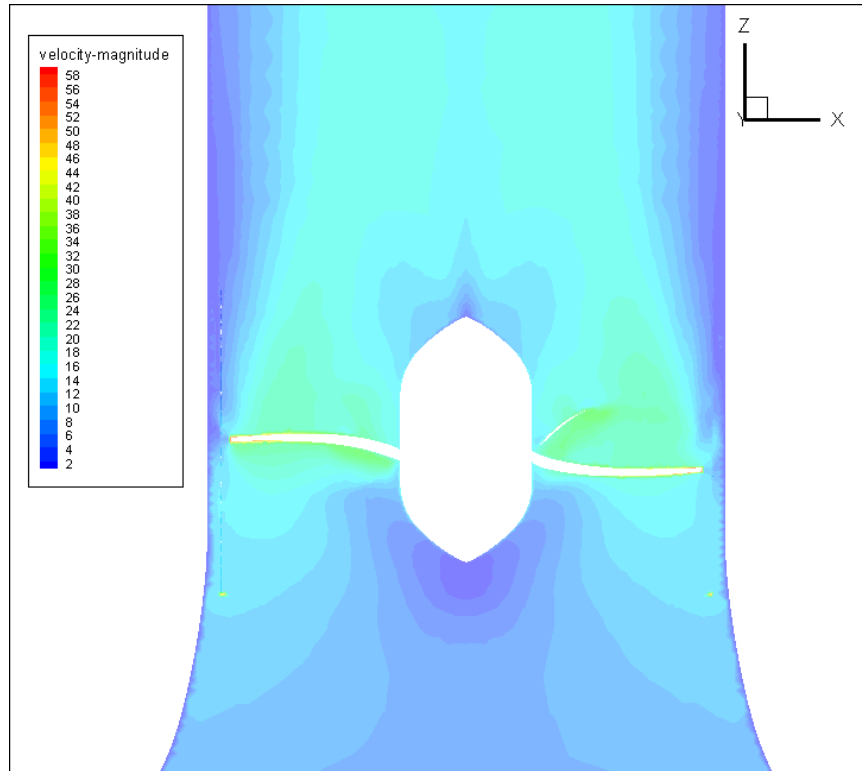
Figure 4.8: Velocity magnitude distribution on XZ plane at 1080 rpm

Fan performance curves are formed for both rotational speeds with flow rate outputs corresponding to pressure rises as seen in Figure 4.9 and Figure 4.10.
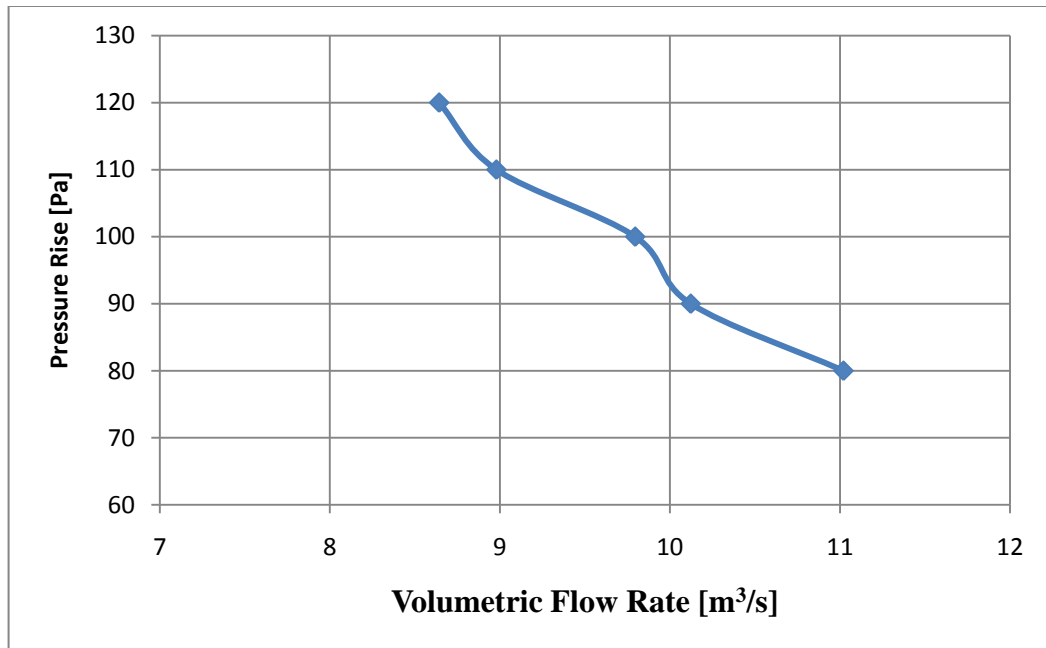
Figure 4.9: Performance curve of the fan at 720 rpm
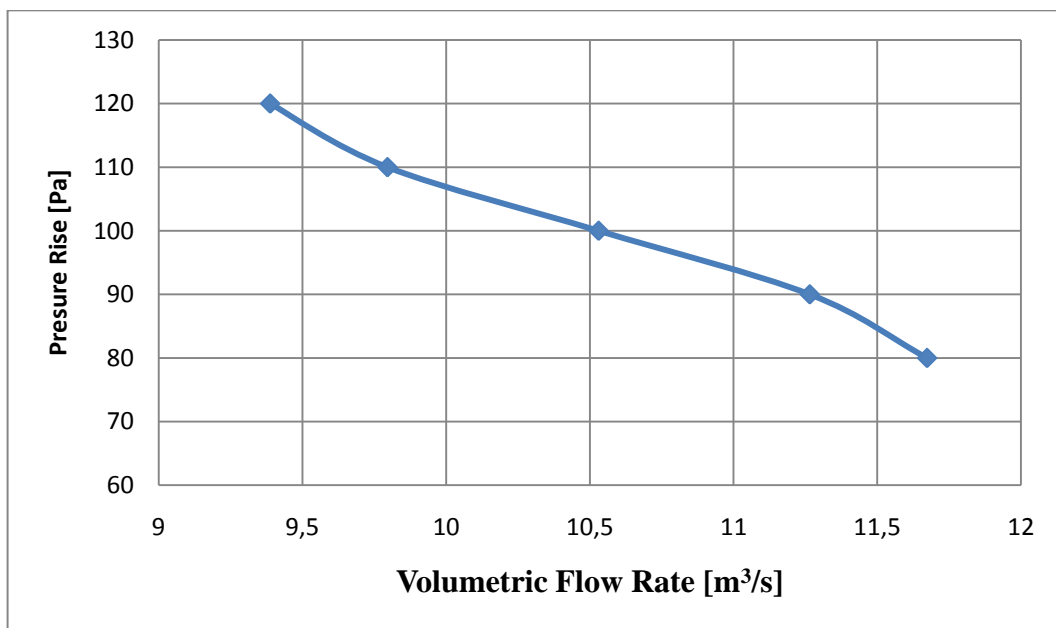
Figure 4.10: Performance curve of the fan at 1080 rpm

4.2. Structural Analysis

Structural analysis is performed to examine the mechanical performance of the fan. Static analysis type of Abaqus/CAE module is used for this test. Since rotor geometry has axial symmetry, only one blade is chosen to be analyzed, instead of using nine blades. Furthermore, to observe deformation, a hinge is located coincident of a blade. After, model is divided into finite elements using Abaqus mesh module.
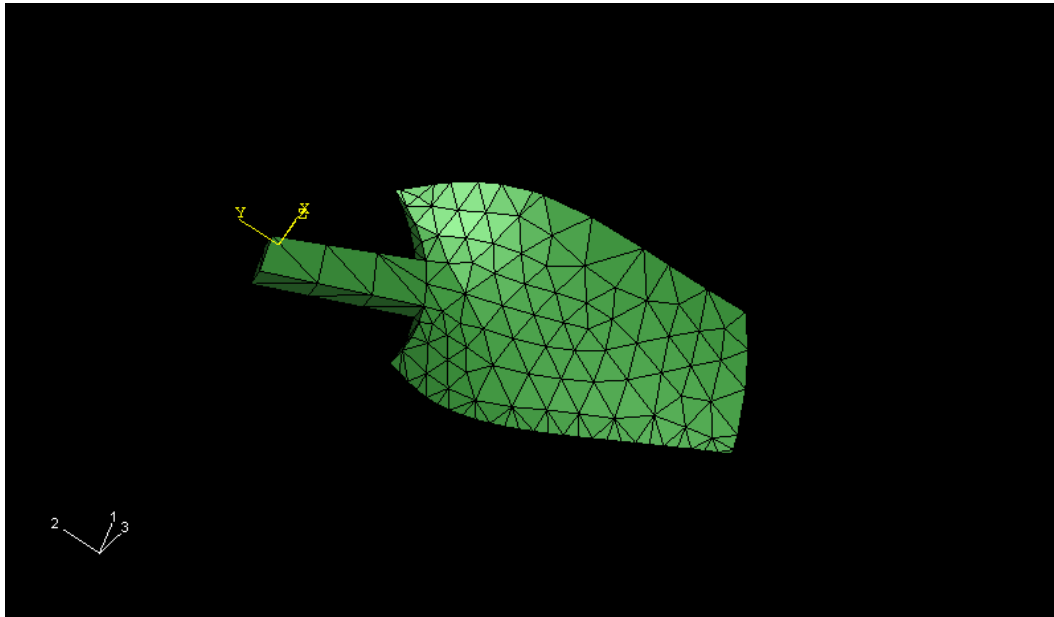
Figure 4.11: The mesh structure of the model

Once meshing step is accomplished, material has been implemented for the modeling; Etal171 which has mechanical properties indicated below is used for manufacturing of the fan.

Table 4.1: Mechanical properties of ETAL171

Elastic Modulus [Gpa]	Poisson Ratio	Density [kg/m3]	Yield Strength [Mpa]	Tensile Strength [Mpa]
2	0,29	2700	48	115

To define boundary conditions, hinge is fixed to the center. Also a uniform 100 Pa load is placed over the surface of the blade as seen in the Figure 4.12. For analysis, the starting point and the start values is defined and only one type of time step is considered.

26
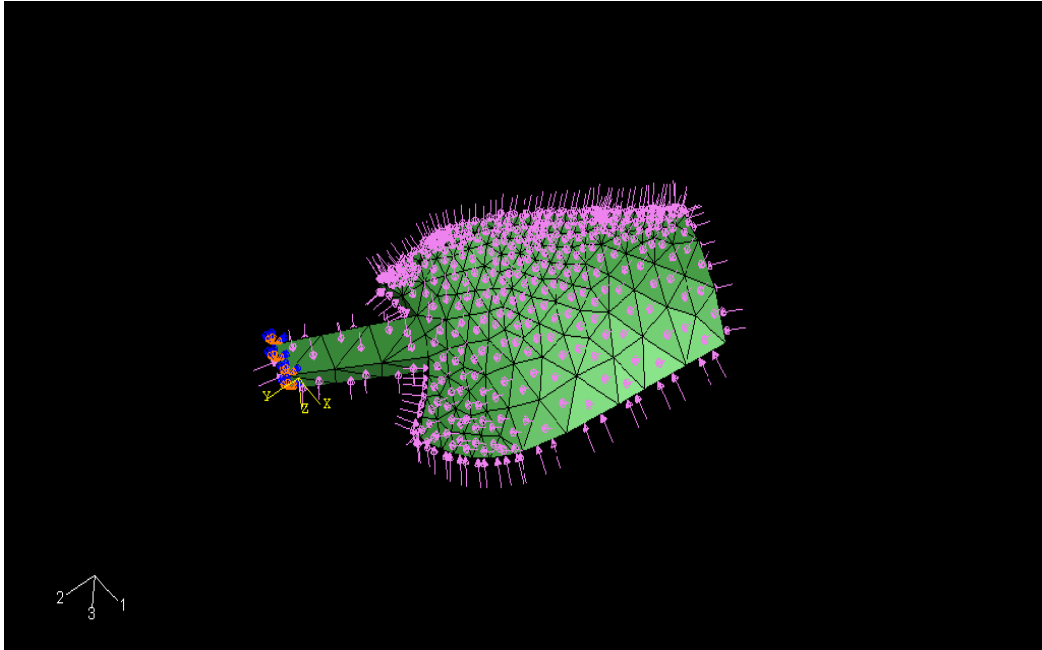
Figure 4.12: Boundary conditions

As a result, since no friction and deformation is noted, it can be said that Etal171 is suitable for fan's endurance.
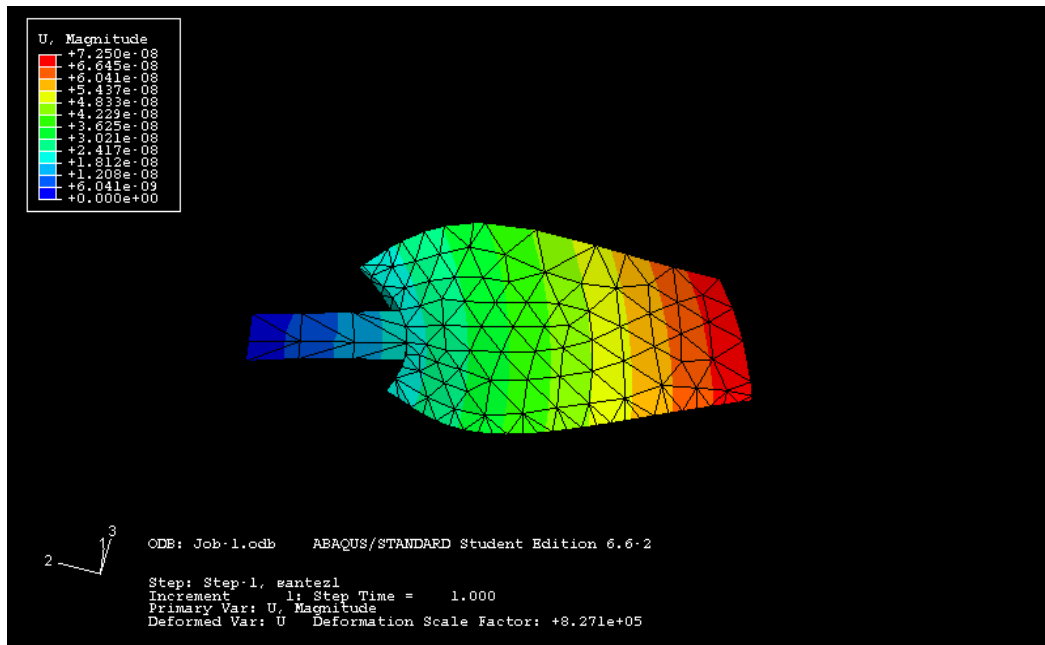
Figure 4.13: Magnitude of displacement distribution on blade
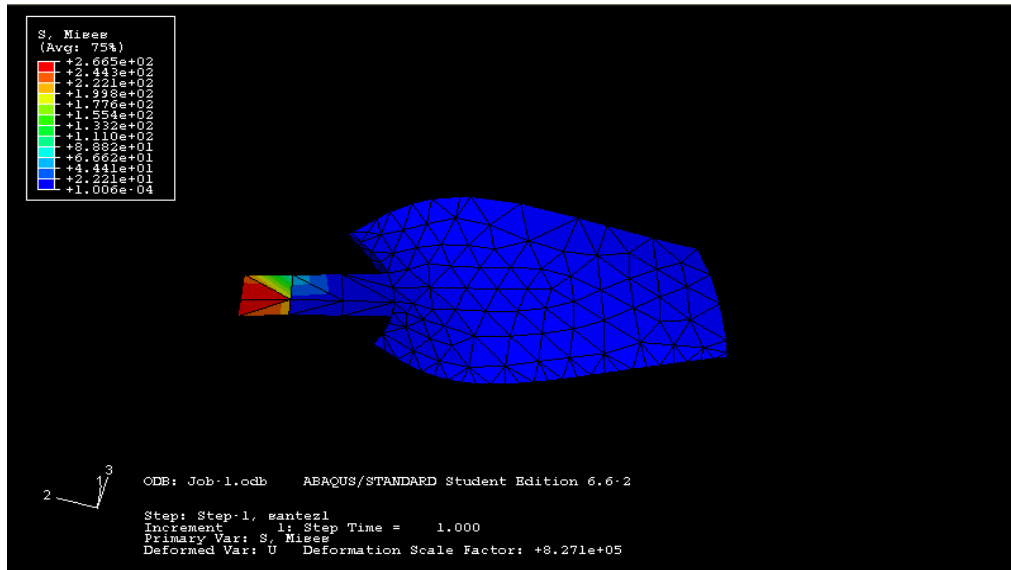
Figure 4.14: Magnitude of stress distribution on blade

REFERENCES

[1] **I. B. Özdemir,** 2010. Private Communication.

[2] **F. Bleier,** 1998. Fan Handbook, McGraw Hill.

[3] **T. Köktürk,** 2005. Design and Performance Analysis of a Reversible Axial Flow Fan, *M.Sc. Thesis*, The Graduate School of Natural and Applied Sciences of Middle East Technical University.

[4] **S.H. Liu, R.F. Huang, C.A. Lin,** 2010. Computational and Experimental Investigations of Performance Curve of an Axial Flow Fan Using Downstream Flow Resistance Method, *Experimental Thermal and Fluid Science* (2010).

[5] **A. Maaloum, S. Kouidri, R. Rey,** 2004. Aeroacoustic Performance Evaluation of Axial Flow Fans Based on the Unsteady Pressure Field on the Blade Surface, *Applied Acoustics*, 65, 367-384.

[6] **B. Eck,** 1973. Fans, Pergamon Press.

[7] **K. Küçükcoşkun,** 2009. Calculations of Flow and Noise Propagation in Centrifugal Fans, *M.Sc. Thesis*, Institute of Science and Technology, Istanbul Technical University.

[8] **E. L. Blades, D. L. Marcum,** 2007. A Sliding Interface Method for Unsteady Unstructured Flow Simulations, *International Journal for Numerical Methods in Fluids,* 53, 507–529.

[9] **G. Constantinesco,** Large Eddy Simulation II 058:0268 Turbulent Flows, 1-5.

[10] **L. Davidson,** 2010. Mechanics of Solids & Fluids. Part II: Fluids Mechanics, Göteborg: Chalmers University of Technology, 43-45.

[11] **S. Pope,** 2000. Turbulent Flows, Cambridge: Cambridge University Press, 110-145.

[12] **M. Germano, et al.,** 1991. A Dynamic Subgrid-Scale Eddy Viscosity Model, *Phys. Fluids* **A, 3,** 1760-1765.

[13] **K.A. Hoffman,Chiang S.T.,** 2000. Computational Fluid Dynamics Vol III, 146–152.

[14] **M. Uygun,** 2004. Turbulence Modeling for Computational Fluid Dynamics, Part 1 Conceptual Outlook, *Journal of Aeronautics and Space Technologies*, **Volume I Number 4**, 20-25.

[15] **S. Kahraman,** 2010. Calculation of Turbulent Flow in a Curved Duct, *M.Sc. Thesis*, Institute of Science and Technology, Istanbul Technical University.

[16] **D. Gizli,** 2009. Calculations of Flow and Noise Propagation in Axial Fans, *M.Sc. Thesis*, Institute of Science and Technology, Istanbul Technical University.

APPENDIX A

PROJECT ORGANIZATION

	WEEKS														
	1	2	3	4	5	6	7	8	9	10	11	12	13	14	
Literature Survey	X	X													Adem Candaş
Solid Model Generation			X	X	X										
Grid Generation					X	X	X								
Structural analysis								X	X	X					
Technical Drawings											X	X			
Writing Thesis												X	X		
Presentation Preparation														X	

	WEEKS														
	1	2	3	4	5	6	7	8	9	10	11	12	13	14	
Literature Survey	X	X													Hasan Erkan Çeliker
Solid Model Generation			X	X	X										
CFD calculations						X	X	X	X						
Technical Drawings										X					
Manifacturing Fan Blade											X	X			
Writing Thesis												X	X		
Presentation Preparation														X	

	WEEKS														
	1	2	3	4	5	6	7	8	9	10	11	12	13	14	
Literature Survey	X	X	X												Ersin Özbalaban
Grid Generation				X	X	X									
CFD calculations						X	X	X	X						
Structural analysis									X	X					
Manifacturing Fan Blade											X	X			
Writing Thesis												X	X		
Presentation Preparation														X	

APPENDIX B

PROJECT COST ANALYSIS

	$ / week	$ / 14 weeks	TL / 14 weeks
Engineering Expenses	750	10.500	16.485
Transportation	30	420	659
Lunch	30	420	659
Others	5	70	110

Software Expenses			
Ansys ICEM CFD v10	10000	10000	15.700
Abaqus/Cae Student Edition	-	-	-
AutoCAD 2010	3000	3000	4.710
Fluent v6.3	10000	10000	15.700

Total		**34.410**	**54.024**

- ✓ Abaqus/Cae Student Edition was provided from computer labs of Faculty of Mechanical Engineering, ITU.

- ✓ Ansys ICEM CFD v10 was provided from BIDB, ITU.

- ✓ AutoCAD 2010 was provided from computer labs of Faculty of Mechanical Engineering, ITU.

- ✓ Fluent v6.3 was provided from BIDB, ITU.

832,67

⌀466,67

416,74

13,46

A

A

A-A Kesit
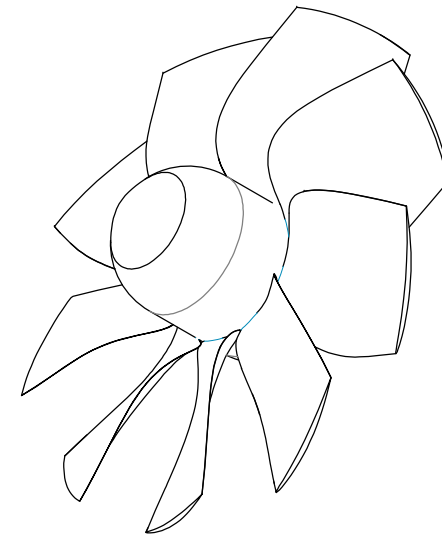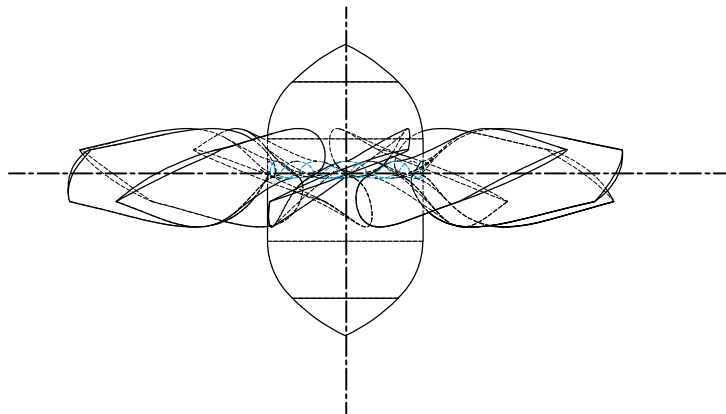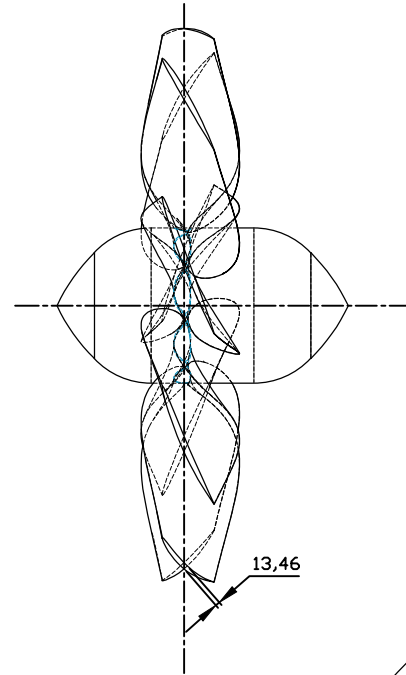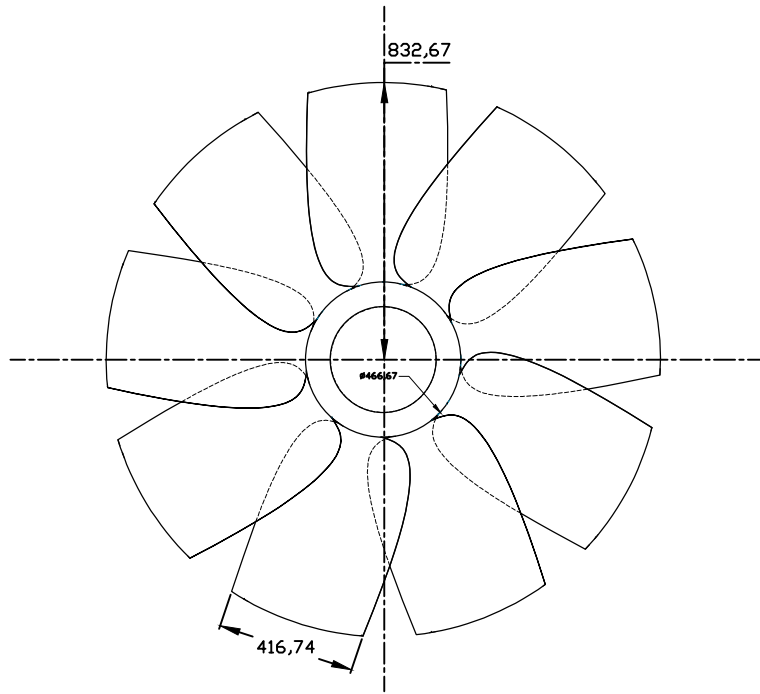
Appendix D - Axial Fan		ISTANBUL TECHNICAL UNIVERSITY FACULTY OF MECHANICAL ENGINEERING			
Scale 1:10	Control	Faculty	Sem	Name - Surname	ID
		Mechanical Engineering	8	Adem Candas	030050019
		Senior Design Project		Due Date	24.05.2010

APPENDIX E

MANIFACTURED FAN BLADE